remote sensing

MDPI

Article

Removing Instrumental Noise in Distributed Acoustic Sensing Data: A Comparison Between Two Deep Learning Approaches

Xihao Gu [1,2], Olivia Collet [1,*], Konstantin Tertyshnikov [1] and Roman Pevzner [1]

[1] Center for Exploration Geophysics, Curtin University, Perth, WA 6845, Australia; guxih@s.upc.edu.cn (X.G.); konstantin.tertyshnikov@curtin.edu.au (K.T.); r.pevzner@curtin.edu.au (R.P.)
[2] School of Geosciences, China University of Petroleum (East China), Qingdao 266580, China
* Correspondence: olivia.collet@curtin.edu.au

Abstract: Over the last decade, distributed acoustic sensing (DAS) has received growing attention in the field of seismic acquisition and monitoring due to its potential high spatial sampling rate, low maintenance cost and high resistance to temperature and pressure. Despite its undeniable advantages, DAS faces some challenges, including a low signal-to-noise ratio, which partly results from the instrument-specific noise generated by DAS interrogators. We present a comparison between two deep learning approaches to address DAS hardware noise and enhance the quality of DAS data. These approaches have the advantage of including real instrumental noise in the neural network training dataset. For the supervised learning (SL) approach, real DAS instrumental noise measured on an acoustically isolated coil is added to synthetic data to generate training pairs of clean/noisy data. For the second method, the Noise2Noise (N2N) approach, the training is performed on noisy/noisy data pairs recorded simultaneously on the downgoing and upgoing parts of a downhole fiber-optic cable. Both approaches allow for the removal of unwanted noise that lies within the same frequency band of the useful signal, a result that cannot be achieved by conventional denoising techniques employing frequency filtering.

Keywords: distributed acoustic sensing (DAS); denoising; machine learning

check for updates

Citation: Gu, X.; Collet, O.; Tertyshnikov, K.; Pevzner, R. Removing Instrumental Noise in Distributed Acoustic Sensing Data: A Comparison Between Two Deep Learning Approaches. *Remote Sens.* **2024**, *16*, 4150. https://doi.org/10.3390/rs16224150

Academic Editors: Andrzej Stateczny and Jaroslaw Tegowski

Received: 5 September 2024
Revised: 24 October 2024
Accepted: 6 November 2024
Published: 7 November 2024

Copyright: © 2024 by the authors. Licensee MDPI, Basel, Switzerland. This article is an open access article distributed under the terms and conditions of the Creative Commons Attribution (CC BY) license (https://creativecommons.org/licenses/by/4.0/).

1. Introduction

Over the last decade, distributed acoustic sensing (DAS) has received growing attention in the field of seismic acquisition and monitoring due to its potential high spatial sampling rate, low maintenance cost and high resistance to temperature and pressure. DAS measures differences in the phase of the backscattered light propagating in a fiber-optic cable and relates these measurements to the axial strain induced on the cable by a propagating seismic wavefield [1]. In recent years, DAS has been successfully applied to near-surface characterization [2], monitoring for CO2 sequestration [3,4] or geothermal [5] projects, volcano monitoring [6] and mining exploration [7]. However, despite its undeniable advantages, DAS faces several challenges, including high noise levels compared to those of conventional seismic sensors [5,8]. A significant portion of DAS data noise, which is typically complex and seemingly random, stems from the optical noise generated by DAS interrogators [9]. Tackling this type of noise, which can be significant in passive data or data acquired with low energy seismic sources, is essential to improve the reliability of DAS for seismic exploration and monitoring.

Signal filtering is one approach that has been used to improve the signal-to-noise ratio (SNR) in DAS data. For instance, Lellouch et al. [10] utilized a straightforward low-pass filter and a 2D median filter to eliminate strong noise from DAS data. More advanced denoising methods such as f-k filters, a curvelet frame [11], a principal component analysis [12] and sparse representation [13] have been applied, with Chen et al. [14] proposing an integrated framework combining several of the individual denoising methods typically

used in seismic data processing. Although these methods yield satisfactory results with optimized parameters, the complexity and spatial non-stationarity of DAS data pose challenges in parameter selection. Manual tuning can lead to incorrect filtering parameters, compromising denoising efficacy and potentially reintroducing false information as valid events [15].

To mitigate the high levels of noise observed in DAS data, several authors have also investigated the use of machine learning. These works can be divided into four categories: supervised learning (SL), weakly supervised learning, self-supervised learning and unsupervised learning. Supervised learning techniques usually require a set of clean/noisy data pairs for training, which can be generated either by adding noise to synthetic data or denoising DAS data using conventional processing techniques [16,17]. When using these techniques, one may encounter several drawbacks: for instance, the synthetic noise that is sometimes added for training the neural network may not capture specific features of DAS noise. On the other hand, ambient noise recorded on the field may contain signals of interest such as microseismic events or ocean microseisms. Hence, training on a dataset created by adding ambient noise to synthetic data may lead to compromising such signals. In this paper, we overcome this issue by introducing a supervised learning methodology in which the training dataset comprises synthetic data and semi-synthetic data consisting of seismic synthetics with real instrumental noise added to them.

Other methods that can be implemented with simple neural network architectures and that do not rely on clean/noisy data pairs for training fall under the category of weakly supervised or self-supervised learning approaches. The self-supervised approach, sometimes referred to as Noise2Void or Noise2Self [18–20], consists of masking a portion of the input data and training the model to predict the missing data. This approach was implemented for DAS data by van den Ende et al. [21] but showed limited effectiveness on data exhibiting high levels of noise.

The weakly supervised learning approach, which is the other method implemented in this paper, is also known as Noise2Noise (N2N) and originates from the work of Lehtinen et al. [22]. This approach circumvents the requirement of having clean/noisy data pairs by training the neural network with data pairs made of two noisy records. Since the noise realizations of the two records making up one pair are assumed to be independent, the neural network is expected to learn the underlying signal but not the noise. By testing their N2N denoising framework on several datasets made of photographs corrupted by different types of noise and magnetic resonance images (MRIs), Lehtinen et al. [22] showed that using noisy/noisy data pairs for training could result in the same denoising performance as using clean/noisy pairs. Two noisy copies of the same signal can be obtained with DAS, provided the fiber-optic cable layout is adequate. For instance, splicing the fiber-optic cable or looping the cable at the bottom of a well can allow for the simultaneous recording of the same signal at almost identical locations. The N2N denoising approach was first applied to DAS data on a fiber-optic cable deployed on the surface of the Rutford Ice Stream in Antarctica [23] and showed promising results. However, they observed some amplitude loss that could be attributed to the fact that the training was performed on data with low-amplitude events and sparse events. In this work, we revisit this methodology to check if training the neural network with higher amplitude events improves upon this amplitude loss. We also train the neural network on datasets acquired downhole with looped fibers, which is a common fiber-optic cable deployment setup.

In the present study, we compare the traditional supervised learning approach (SL) and the weakly supervised learning approach (N2N). The paper outline is as follows: we first describe the DAS noise characteristics and the generation and pre-processing of the training datasets used for both methods before providing details on the neural network's architecture, training and application; then, in the results section, we assess the generalizability of our denoising neural networks by testing them on semi-synthetic data and on field data, including active and passive DAS seismic data acquired downhole. Finally, in the discussion section, we highlight the benefits and limitations of both approaches and

benchmark them against two other denoising methods: a conventional bandpass filter and a neural network trained with data pairs made of denoised/noisy data pairs.

2. Methods

2.1. Hardware Noise Characteristics

DAS data contain several types of optical noise, which are inherent to the interrogator unit [9]. To investigate the instrument noise pattern, we recorded ambient noise on a 500 m long acoustically isolated coil of fiber for 5 days in a laboratory environment. The acoustically isolated coil consists of a fiber-optic cable encased in a metal box and suspended over the ground to isolate it from external vibrations. As such, it provides a good proxy for the DAS instrumental noise. For this study, noise data were acquired with Silixa iDAS v2 interrogator unit with a 10 m gauge length, a 1 m channel spacing and a temporal sampling rate of 1 ms. Figure 1a displays an example of a 512 ms long noise recording. This noise record illustrates the complexity of DAS noise and clearly exhibits two components: a seemingly random noise and a vertical noise present on contiguous channels. Note that this noise pattern varies for each type of DAS interrogator unit. Figure 1b displays the corresponding spectral density computed with Welch's method [24]. The noise level shows a steady increase with increasing frequency. The aim of measuring the instrument's noise floor using the acoustically isolated coil is twofold: first, we add this instrument noise to the seismic synthetics in order to generate semi-synthetic data with realistic instrument noise for training and testing purposes, and second, we compare the noise removed after denoising to the recorded instrument noise.

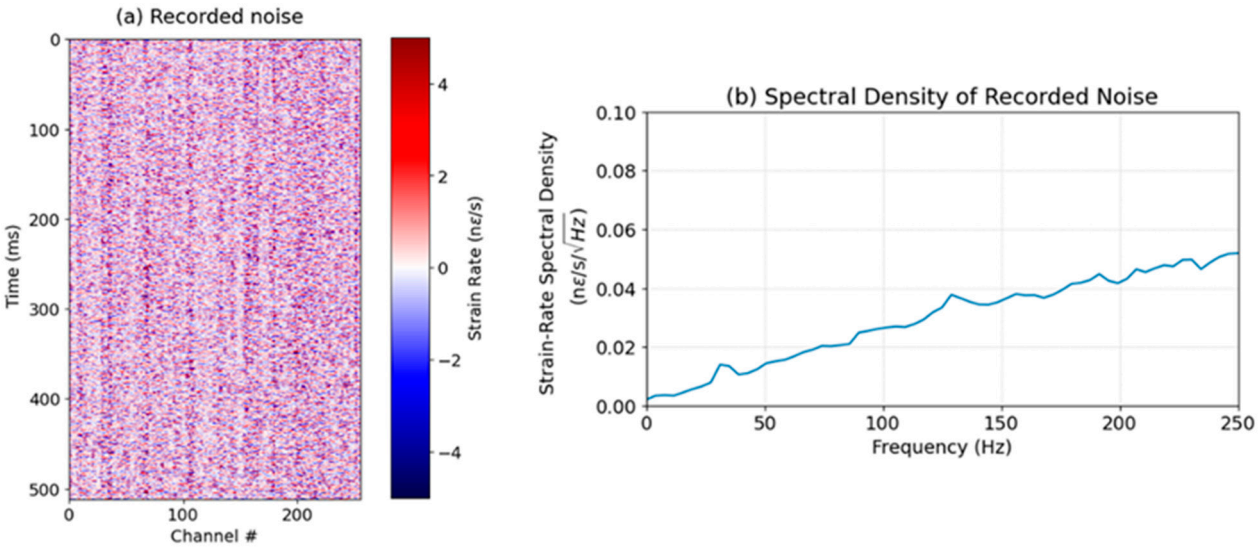


Figure 1. (**a**) Noise recorded on an acoustically isolated coil of fiber; (**b**) corresponding strain rate spectral density.

2.2. Training Datasets

2.2.1. Semi-Synthetic Training Dataset

A well-labeled and realistic training set is essential to effectively train a neural network through supervised learning. Herein, we describe the methodology used for generating the training set (Figure 2). Initially, we derive the velocity model from sonic and density logs acquired in CRC-3 well at the CO2CRC Otway test center [25]. Subsequently, we conduct 1.5D full-wave numerical simulations for a vertical point source emitting a 160 Hz central frequency Ricker wavelet using the Ocean Acoustics and Seismic Exploration Synthesis (OASES) software (Version 3.1) [26]. The synthetics are generated for an offset vertical seismic profile (VSP) geometry with source offsets ranging from 10 to 3000 m with a step of 10 m, and receiver depths varying between 50 and 1650 m with a separation of 100 m. As OASES outputs particle velocity, we subtract channels and normalize by the gauge length

to convert the output to strain rate for the same gauge length as in the DAS interrogator used in this study. From these synthetics, we generate a set of 100 clean DAS data instances, denoted as y_i, where i indicates the sample index, each data instance comprising 256 traces with 512 time samples with a sampling rate of 1 ms. These clean data instances serve as target data for training the neural network. In parallel, we generate a corresponding set of 100 noise data instances, referred to as n_i, of identical dimensions. These noise data instances are normalized and then added to their corresponding clean counterparts to generate the semi-synthetic dataset x_i, which can be expressed as follows:

$$x_i = a_i y_i + n_i. \tag{1}$$

Note that in Equation (1), no summation is implied over repeated indices. In order to generate semi-synthetic data with different SNR values, we normalize the simulated data relative to their maximum amplitude by applying a scaling factor a_i, which varies randomly between 0.8 and 3. The ultimate objective of the denoising task is to reconstruct the clean signal y_i from the observed data x_i.

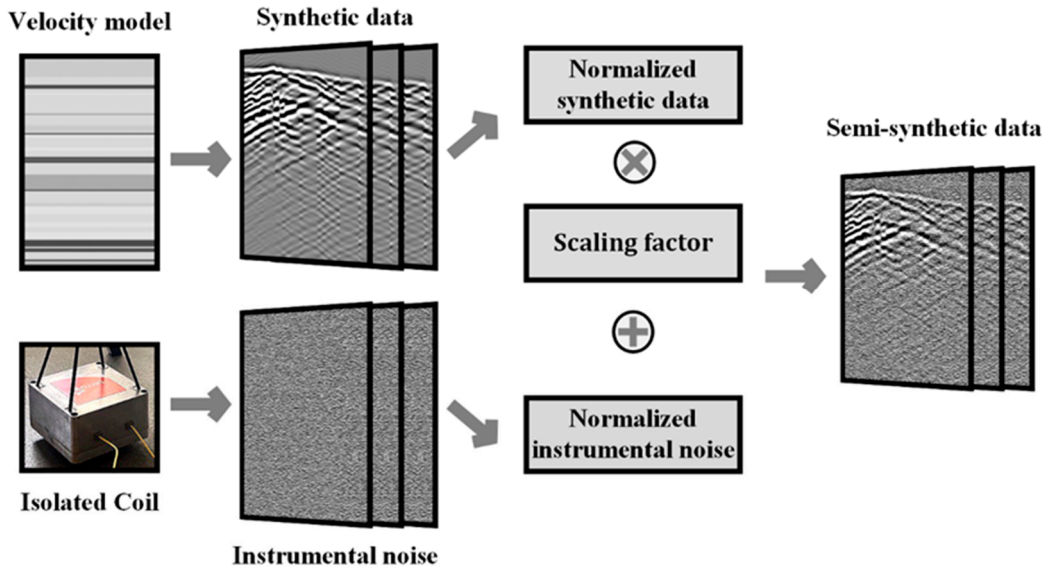


Figure 2. Flowchart for constructing semi-synthetic DAS data using synthetic data and recorded instrumental noise.

In this study, we employ a supervised learning framework to extract features from large-scale DAS data. The use of convolutional neural networks with fixed kernel sizes is computationally efficient, but it may result in insufficient feature extraction on large-scale datasets. To address this limitation, we employ a patching process, dividing the large 2D DAS dataset into smaller patches. Subsequently, an unpatching step is employed to reconstruct the initial 2D DAS dataset from these processed patches. This unpatching process incorporates Hann windows [27], which weigh the overlapping blocks, enabling the extraction of local information with some degree of redundant overlap. Each patch is defined by two parameters: patch size and overlap size. We set the patch size to 128 × 96 and the overlap size to 64 × 48, yielding 2700 patches from the original 100 semi-synthetic records.

2.2.2. Noise2Noise Training Dataset

To train the neural network following the N2N method, we use DAS VSP data acquired using a 45 kg accelerated weight drop source at the Curtin National Geosequestration Laboratory (NGL) well facility [28]. The 900 m deep well is equipped with a looped single-mode fiber-optic cable cemented behind fiberglass casing [29] (Figure 3). A series of 205 shots were emitted from a fixed shot point located 165 m away from the wellhead and

recorded using a Silixa iDAS v2 interrogator with a 10 m gauge length, 1 m channel spacing and 16 kHz pulse repetition frequency downsampled to 1 kHz. An example of a raw shot record is displayed in Figure 4 (left panel). Channels 480–2260 show the signal recorded on the fiber-optic cable cemented behind the casing. Since the fiber is looped at the bottom of the well, we observe a clear symmetry of the signal recorded on the downgoing and upgoing parts of the fiber-optic cable.

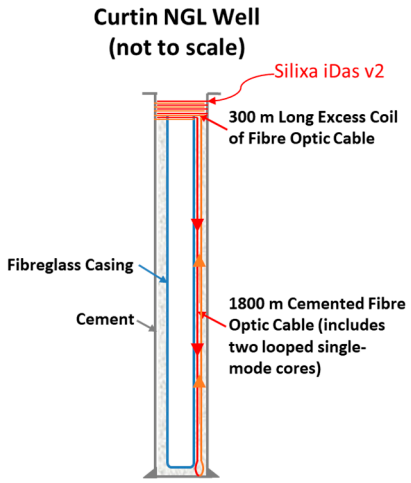


Figure 3. Schematics of the borehole optic cable used for the acquisition of the Noise2Noise training dataset. The cable is looped at the bottom of the well; the downgoing and upgoing parts of the cable are depicted in red and orange, respectively.

The idea of the N2N approach is to train the neural network using two copies of the same signal with different noise realizations. Here, these two copies are provided by the data acquired on the downgoing and upgoing parts of the fiber. Hence, we split each shot record into two records corresponding to the downgoing and upgoing parts of the fiber. To align the depths of the records, we determine the channel mapping that minimizes the RMS amplitude difference between the downgoing and upgoing records (Figure 4). After splitting the record and flipping the target data (upgoing part of the fiber), we obtain two records of the same wavefield but with different noise realizations. Then, to normalize the data, we remove the mean (across all channels) and divide it by the standard deviation. Finally, we segment this training dataset into patches with a size of 128 samples $\times$ 96 channels to reduce computational cost while still preserving the ability to extract waveform features. Similar to the SL approach data preparation described above, these patches are extracted with an overlap of half their size to avoid edge artefacts when reconstructing the denoised images. For the training, we use 200 shot records, which corresponds to 49,400 patches.

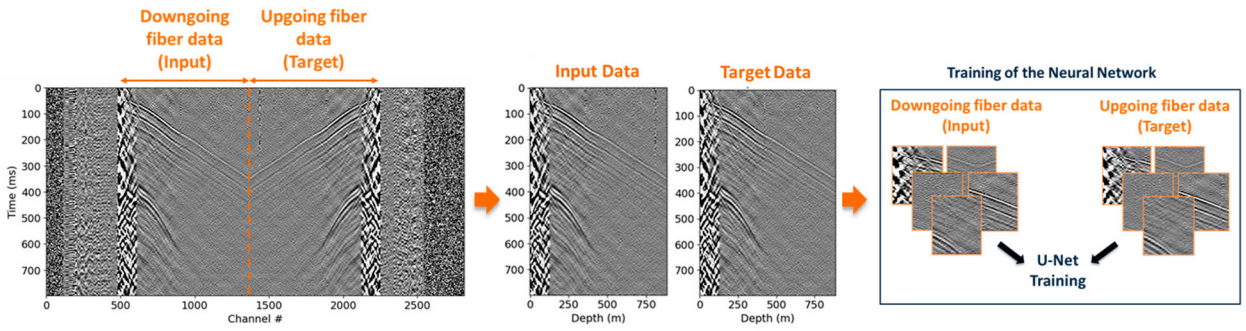


Figure 4. Illustration of the data preparation workflow and neural network training for the N2N approach.

2.3. Neural Network Architecture and Training

In this study, we adopt the methodology employed by Lapins et al. [23] who denoised DAS data by training a UNet-type neural network with very few layers. A summary of the neural network used to perform deep learning denoising in this study is given in Table 1. UNet networks rely on "encoder–decoder" architectures. The encoder blocks perform downsampling, while the decoder blocks perform upsampling. UNets have the advantage of combining high-resolution and low-resolution features through the skip connection layers, which makes them ideal and computationally efficient for image denoising [30]. The training process consists of deriving a non-linear relationship between the input and output data:

$$\hat{y}_i = \mathcal{F}_\theta(x_i), \tag{2}$$

where the mean squared error (MSE) loss function that is minimized during the training process is expressed as follows:

$$\mathcal{L}(\theta) = \underset{\theta}{\operatorname{argmin}} \sum_{i=1}^{N} [\mathcal{F}_\theta(x_i) - a_i y_i]^2, \tag{3}$$

where N is the number of input–target training pairs in a batch set, and y_i is the target clean data. To speed up convergence, the model weights are updated using the Adam optimization algorithm [31]. The network is trained for 250 epochs, with a learning rate set to linearly decrease from 10^{-3} to 10^{-5} with increasing epochs.

Table 1. The neural network used to perform deep learning denoising in this study.

Layer (Type)	Output Shape	Param #	Connected to
input_1 (InputLayer)	(128, 96)	0	[]
reshape (Reshape)	(128, 96, 1)	0	[input_1]
conv2d (Conv2D)	(128, 96, 24)	240	[reshape]
leaky_re_lu (LeakyReLU)	(128, 96, 24)	0	[conv2d]
max_pooling2d (MaxPooling2D)	(64, 48, 24)	0	[leaky_re_lu]
conv2d_1 (Conv2D)	(64, 48, 48)	10,416	[max_pooling2d]
leaky_re_lu_1 (LeakyReLU)	(64, 48, 48)	0	[conv2d_1]
up_sampling2d (UpSampling2D)	(128, 96, 48)	0	[leaky_re_lu_1]
concatenate (Concatenate)	(128, 96, 72)	0	[up_sampling2d]
conv2d_2 (Conv2D)	(128, 96, 48)	31,152	[concatenate]
leaky_re_lu_2 (LeakyReLU)	(128, 96, 48)	0	[conv2d_2]
conv2d_3 (Conv2D)	(128, 96, 24)	10,392	[leaky_re_lu_2]
leaky_re_lu_3 (LeakyReLU)	(128, 96, 24)	0	[conv2d_3]
conv2d_4 (Conv2D)	(128, 96, 1)	25	[leaky_re_lu_3]
reshape_1 (Reshape)	(128, 96)	0	[conv2d_4]

52,225 trainable parameters.

For the N2N approach, we use the same shallow UNet type of architecture. However, unlike the traditional supervised approach, the input/target pair used for the N2N neural network training is made of two noisy records x and x':

$$\begin{aligned} x &= y + n, \\ x' &= y + n', \end{aligned} \tag{4}$$

where n and n' are two different noise realizations, and y is the underlying clean signal. In this case, the MSE loss function to be minimized during the training process is expressed as follows:

$$\mathcal{L}(\theta) = \underset{\theta}{\operatorname{argmin}} \sum_{i=1}^{N} \left[\mathcal{F}_\theta(x_i) - x_i^{'} \right]^2, \tag{5}$$

where $\mathcal{F}_\theta$ denotes the network architecture, θ refers to the model parameters, i is the training sample index and N is the number of input–target training pairs in a batch set. By expanding the MSE in Equation (5), the loss function is reduced to the one used in traditional supervised learning if the noise realizations are independent [32]. During the training process, we used the same optimization algorithm and learning rate scheme as the one for the traditional supervised learning training.

2.4. Neural Network Application

After training, the denoising neural networks can be applied to raw DAS records acquired with the same type of interrogator and similar acquisition settings as the noise recordings or the field data used in the training datasets for the SL and N2N methods, respectively. For borehole DAS data, the neural network input can be the data recorded on the downgoing part of the fiber, the upgoing part of the fiber or a stack of both to further improve the SNR. The input data should be normalized and segmented into overlapping patches similar to the pre-processing applied to the input training data. To avoid artefacts due to the segmentation into patches, when reconstructing the full denoised records, we apply weights computed from Hann windows on the overlapping patches [27].

2.5. Performance of the Network: SNR Computation

SNR is one of the important indicators to measure the quality of seismic data, and it is also an important indicator for evaluating the performance of denoising methods. In this study, we compute SNR attribute sections quantifying the signal coherency based on the approach described in Hatton et al. [33]. Assuming the noise is additive, uncorrelated and zero-mean, the SNR can be estimated between pairs of traces in a given time window using the following equation:

$$SN_j = \sqrt{\frac{\left[g_{j,j+1}\right]_{\max}}{1 - \left[g_{j,j+1}\right]_{\max}}}, \tag{6}$$

where j is the trace number, $g_{j,\,j+1}$ is the normalized cross-correlation between traces j and $j+1$ and $\left[g_{\,j,\,j+1}\right]_{\max}$ is the maximum cross-correlation value. Intuitively, signals corrupted with high levels of random noise will yield lower SNR values than signals recorded with low noise levels. In addition to these SNR attribute sections, we calculate the average SNR on the entire gather by cross-correlating consecutive traces on the full record length and averaging the maximum cross-correlation values. The obtained values are shown at the top of the figures of SNR sections (e.g., Figure 5e–g).

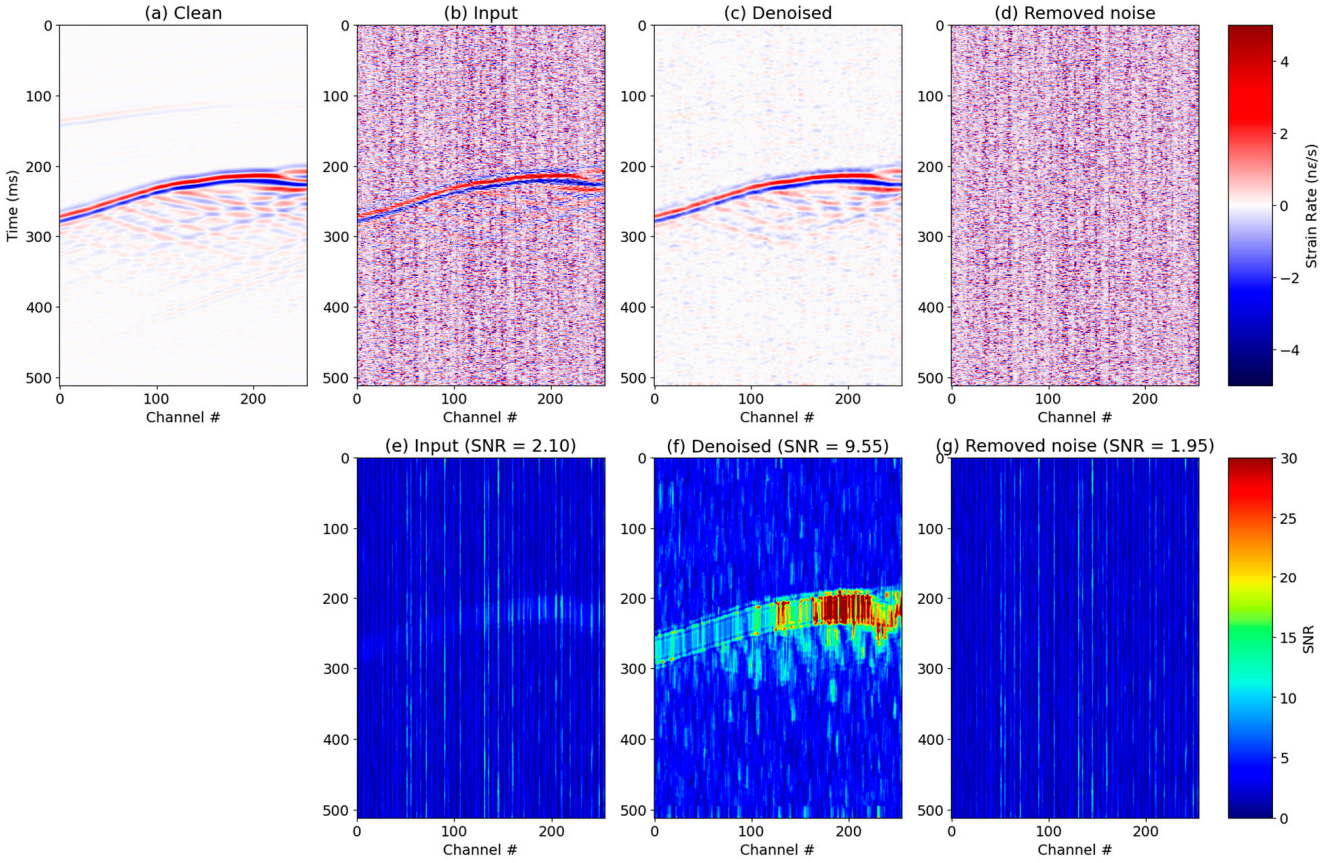


Figure 5. Denoising performance of the SL neural network trained on semi-synthetic data. (**a**) Clean data, (**b**) input semi-synthetic data, (**c**) denoised result and (**d**) removed noise. To quantitatively assess the denoising performance, SNR sections are computed for (**e**) the input data, (**f**) the denoised result and (**g**) the removed noise. SNR values at the top of the plots indicate the average SNR value for the corresponding section.

3. Results

In this section, we demonstrate the validity and effectiveness of the pre-trained supervised learning (SL) and Noise2Noise (N2N) neural networks on synthetic and field data examples.

3.1. Application to Synthetic Dataset

To assess the denoising capabilities of the trained neural networks, we first test their performance on one of the semi-synthetic gathers that were used to train the SL neural network.

3.1.1. Neural Network Trained on Semi-Synthetic Dataset

Figure 5a–d display the clean data, input semi-synthetic data, denoised result and removed noise using the SL-trained neural network. The corresponding SNR sections quantitatively evaluating the denoising network are shown in Figure 5e–g, respectively. As observed in Figure 5b, the amplitude of the VSP wavefield components varies throughout the section, with the weaker P-wave arriving first, followed by the stronger S-wave signal. The denoising process improves the continuity of the VSP wavefield; however, the neural network does not recover the amplitudes of the P-wave arrivals due to their similar magnitude to the noise. Nevertheless, the denoising network successfully retrieves weaker events below the S-wave arrival. The removed noise section (Figure 5d) shows the background noise that is suppressed by the denoising algorithm. This noise not only contains strong random noise, but also high-intensity trace noise over multiple channels (vertical stripes).

The visual comparison between the input and the denoised sections, and the analysis of the removed noise section, constitute the first tools in validating the methodology and assessing the neural network performance. To estimate the denoising performance more quantitatively, we compute the average SNR and the SNR attribute sections that quantify the correlation between traces. The analysis of the SNR sections shown in Figure 5e–g reveals that our method effectively eliminates the majority of noise from the input data, significantly augmenting the SNR of the input data (from 2.10 to 9.55). At the same time, the removed noise contains little coherent energy, with minimal damage to the useful signal.

Figure 6 shows the strain rate spectral densities of the input data, clean data, denoised result, removed noise and recorded noise. There are some disparities between the removed noise and the recorded noise, which would require further investigation. We also note a small mismatch between the amplitude spectra of the denoised and clean data. However, the spectra are very consistent, up to 50 Hz.

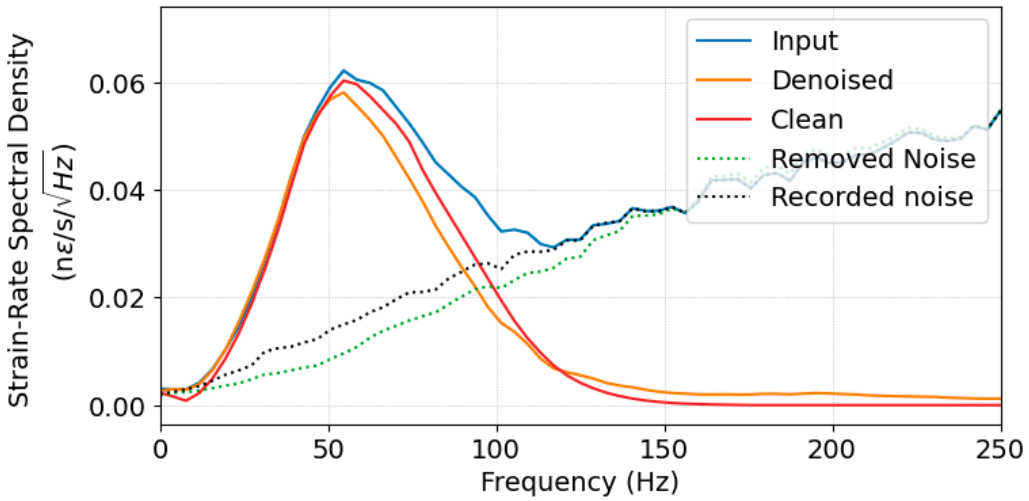


Figure 6. Comparison of strain rate spectral densities calculated for the input data (blue line), clean data (red line) and the data denoised using the SL network trained on semi-synthetic data (orange line). The removed noise (green dotted line) and the noise recorded on an acoustically isolated coil (black dotted line) are also displayed. The corresponding gathers for the data are shown in Figure 4.

3.1.2. Noise2Noise Trained Neural Network

To test the performance of the N2N-trained neural network, we use the same semi-synthetic example. Figure 7a–d shows the clean, input, denoised and removed sections for the selected gather. Again, the denoising allows us to better distinguish the previously masked signal. The analysis of the corresponding SNR attribute sections (Figure 7e–g) demonstrates further evidence of the N2N network's ability to remove noise, with an average SNR value increasing from 2.10 to 10.89. We also note a close match between the spectral densities of the removed noise and the recorded noise added to the synthetic data to generate the semi-synthetic input (Figure 8). However, there seems to be some signal leakage, with the denoised data lacking some of the high-frequency content present in the clean data, as shown by the mismatch in the spectral densities of the denoised data and clean data between 40 and 120 Hz (Figure 8). The loss of high frequencies may arise from the lack of high frequencies in the training dataset used for the N2N approach, with the weight drop source employed for the training dataset having a dominant frequency of 70 Hz (Figure 11) and with most of the signal lying in the [20, 70] Hz frequency band. This issue is further illustrated in the discussion section.

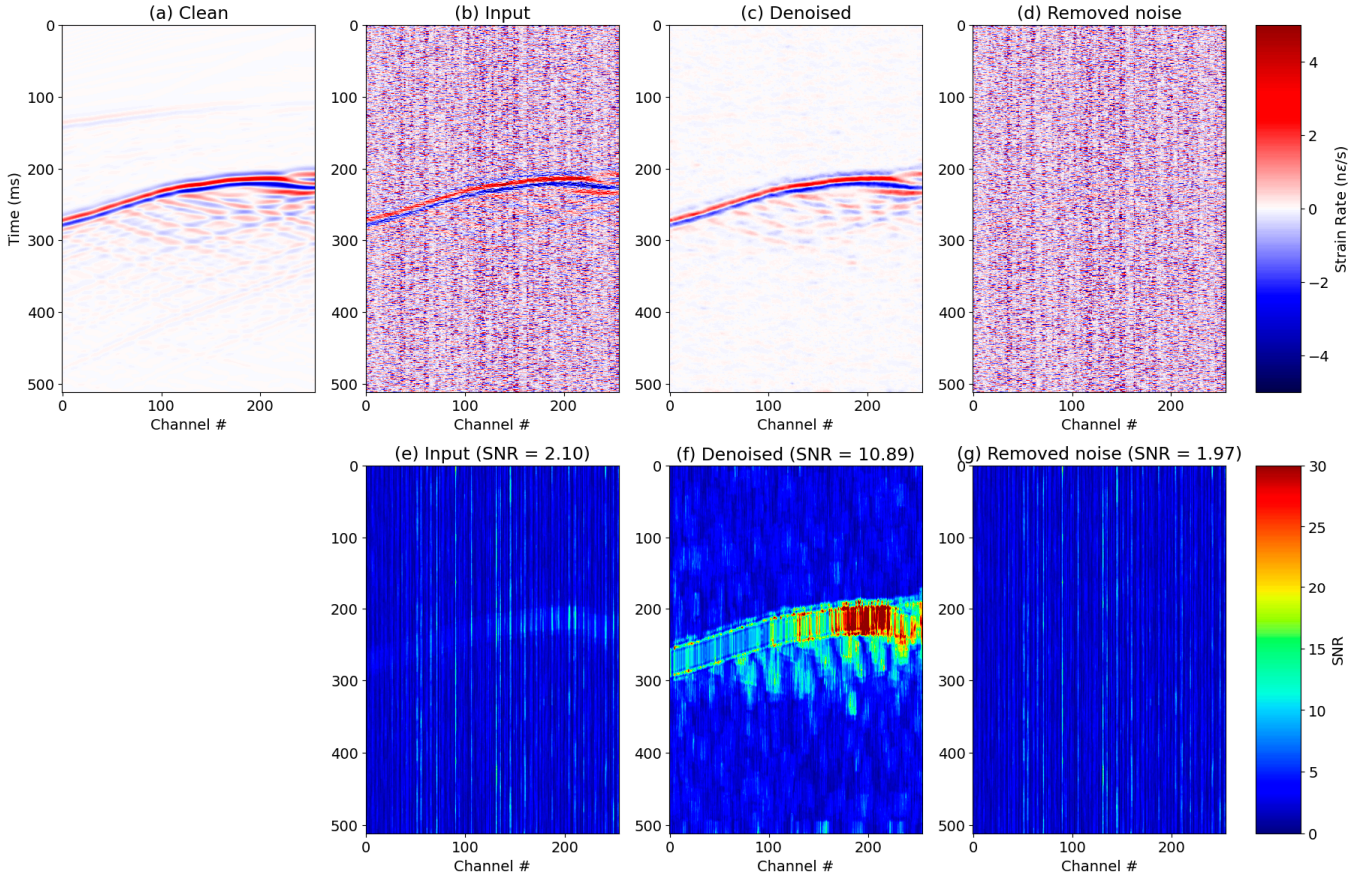


Figure 7. Denoising performance of the N2N-trained neural network on the Otway semi-synthetic dataset: (**a**) clean data, (**b**) input gather, (**c**) denoised result and (**d**) removed noise. Corresponding SNR attribute sections are shown in panels (**e**–**g**). The average SNR values are displayed on top of each section.

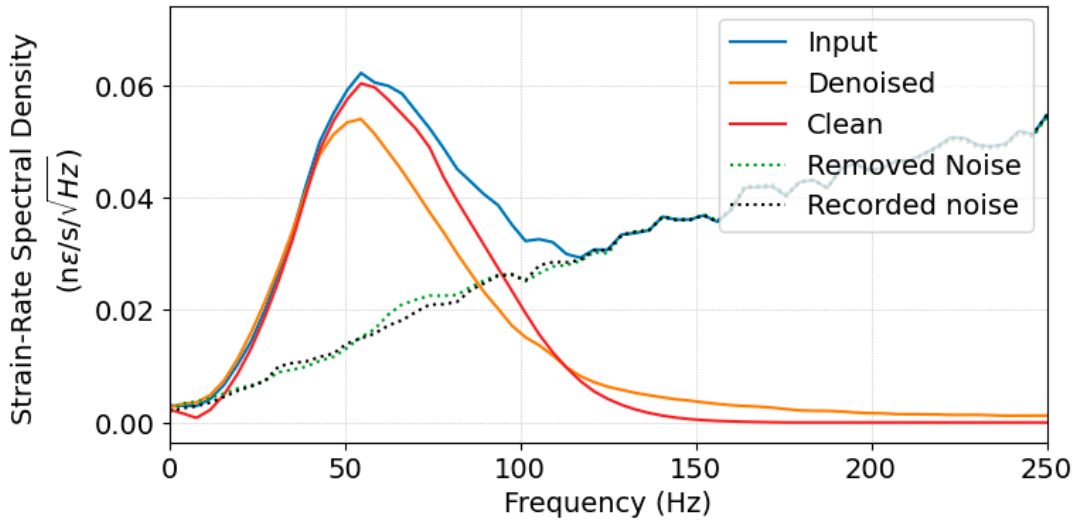


Figure 8. Strain rate spectral densities of the noisy input (blue line), N2N-denoised (orange line), and clean input (red lines) data for the Otway semi-synthetic record example. The spectral densities of the removed noise (dotted green line) and the recorded noise (dotted black line) that were originally added to the clean synthetic data are also compared.

3.2. Application to Low-Power Active-Source DAS-VSP Dataset

The DAS-VSP dataset used in this section is the dataset acquired with a small weight-drop source at the NGL well, which was used to train the N2N neural network.

3.2.1. Neural Network Trained on Semi-Synthetic Dataset

The input raw DAS shot gather displayed in Figure 9a exhibits a substantial level of noise, significantly compromising the coherency of the P- and S-wave arrivals and their multiples. Following the denoising process, the data in Figure 9b unveil previously imperceptible small-amplitude signals that were challenging to discern in the original input data. Notably, in the input data, the amplitude of the direct P-wave is comparable to the level of ambient noise after channel 400, while it is visible down to the bottom of the well in the denoised data.

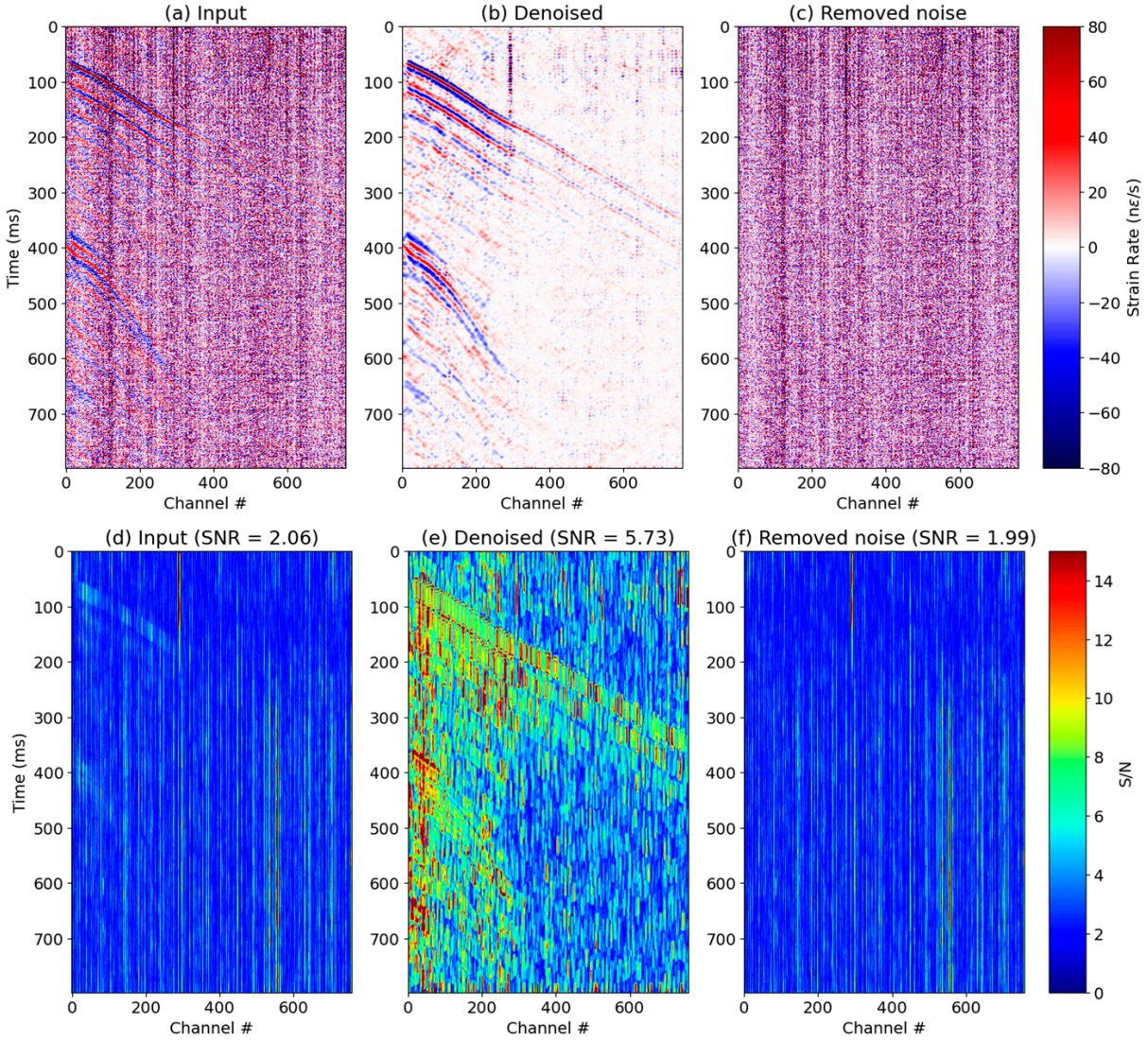


Figure 9. SL neural network application to the DAS-VSP data acquired with a low-power active source: (**a**) raw DAS shot record, (**b**) denoised result and (**c**) removed noise. The corresponding SNR sections are shown in figures (**d**–**f**). SNR values at the top of the plots indicate the average SNR value for the corresponding section.

Moreover, the absence of pronounced signal leakage in the removed noise (Figure 9c) suggests that the useful signal is preserved during the denoising process. To quantitatively evaluate the denoising capabilities of the supervised network on the NGL field data, we

computed the SNR sections for the input data (Figure 9d), denoised result (Figure 9e) and removed noise (Figure 9f). Compared to the SNR of the input data, the significantly elevated SNR values of the denoised result indicate the effectiveness of our proposed neural network. Finally, Figure 10 presents the strain rate spectral densities of the input data, denoised result and removed noise for the NGL well data example. In contrast to the spectral density of the semi-synthetic data shown in Figure 6, the NGL DAS data exhibit multiple spectral peaks, which highlights the complexity of field data. This implies that the denoising result achieved by our network cannot be replicated through straightforward bandpass filtering alone.

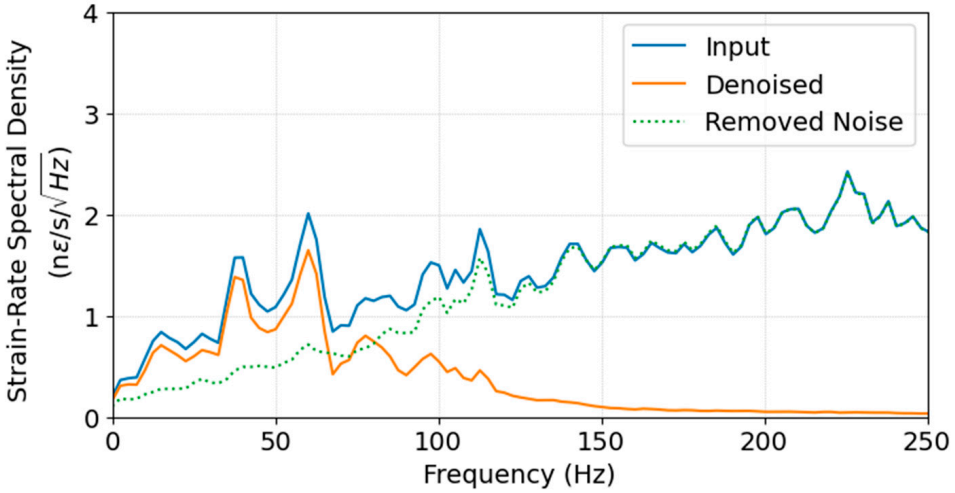


Figure 10. Comparison of strain rate spectral densities calculated for the input data (blue line), the data denoised using the SL supervised network (orange line) and the removed noise (dotted green line). The corresponding gathers for the input data, denoised data and removed noise data are shown in Figure 9.

3.2.2. Noise2Noise Trained Neural Network

Figure 11 shows the same DAS-VSP shot gather denoised using the DAS N2N approach. The denoised data (Figure 11b) exhibits a decrease in the intensity of the seemingly random background noise and the channel noise (vertical streaks) compared to the raw DAS data (Figure 11a). This observation is confirmed by the removed noise section (Figure 11c). Similar to the SL-denoising neural network result, we discern the first P-wave arrival down to the bottom of the well after applying the neural network.

The average SNR computed on the shot gather shown in Figure 11 increases from 2.06 for the input raw data to 4.87 for the N2N-denoised data. Figure 11e–f show the SNR sections obtained from the raw data, denoised data and removed noise. From the denoised data section, we observe an improved signal coherency.

Finally, we calculate the strain rate spectral densities of the input, denoised and removed noise sections using Welch's method [24]. Figure 12 shows the spectral densities corresponding to the shot gathers displayed in Figure 11. We observe that between 70 Hz and 100 Hz, the spectral density of the removed noise (green dotted line) reaches the same level as the spectral density of the input signal (blue solid curve), which highlights the difficulty in removing such noise with frequency filtering only.

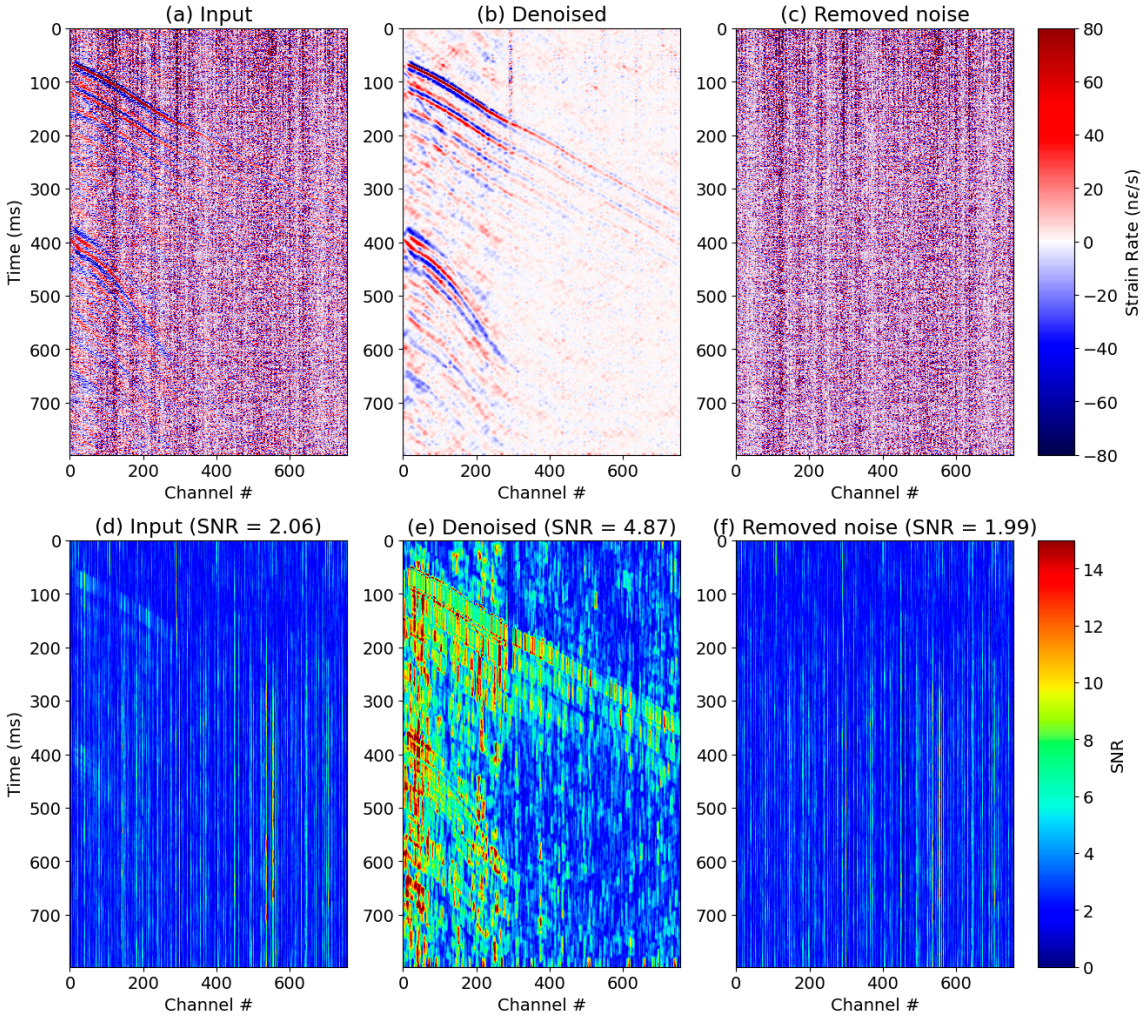


Figure 11. N2N neural network application to the DAS VSP data example used in training: (**a**) raw DAS shot record, (**b**) denoised result and (**c**) removed noise. The corresponding SNR sections are shown in figures (**d**–**f**). SNR values at the top of the plots indicate the average SNR value for the corresponding section.

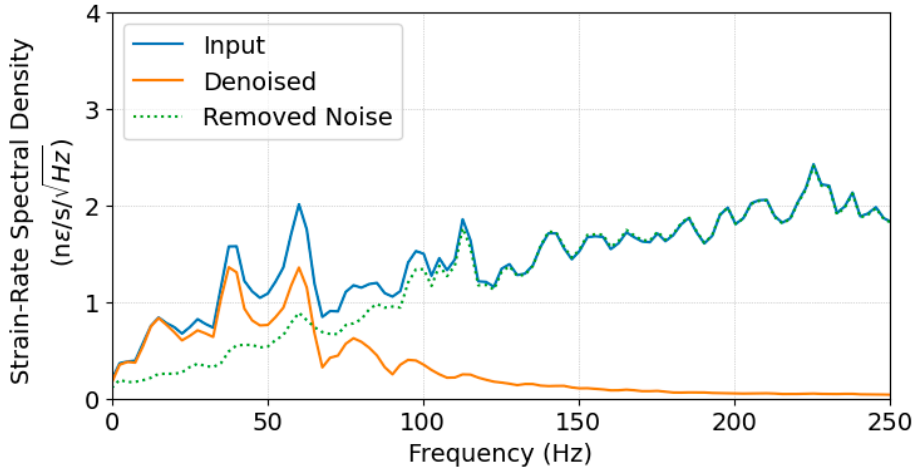


Figure 12. Comparison of strain rate spectral densities calculated for the input data (blue line), the data denoised using the N2N approach (orange line) and the removed noise (green dotted line). The corresponding gathers for the input data, denoised data and removed noise data are shown in Figure 11.

3.3. Application to Microseismic Events

In recent years, DAS technology has been extensively trialed at the Otway International Test Centre, an onshore carbon capture and storage (CCS) test site located in the Australian state of Victoria, approximately 240 km west of Melbourne, primarily for monitoring carbon dioxide storage through VSP [25]. DAS arrays have been installed in several monitoring wells, enabling active and passive continuous monitoring. Beyond their primary purpose of CO_2 storage monitoring, continuous DAS acquisition also provides insights into induced seismic signals arising from CO_2 injections [34]. However, DAS noise may contaminate passive seismic records and subsequently impact microseismic event detection, localization and characterization. Hence, we tested our pre-trained models, aiming to denoise a microseismic event recorded in February 2021. The event was recorded in the CRC-7 well, an observation well equipped with constellation fiber connected to a Silixa iDASv3 interrogator. The data were acquired with a 1 ms sample rate, 1 m channel spacing and 10 m gauge length.

3.3.1. Neural Network Trained on Semi-Synthetic Dataset

As illustrated in Figure 13a, the input data exhibits various seismic wave components, including direct P- and S-waves, converted waves and reflected waves. In addition, it captures the low-frequency Rayleigh waves generated by ocean microseisms [35,36], which are particularly visible as the low-frequency blue component in the shallow part of the well (channel numbers above 1000). The input record is contaminated by vertical and random noises, which are effectively reduced by the algorithm, as shown in the denoised section (Figure 13b). The denoising neural network also enhances low-amplitude signals corresponding to reflected and scattered waves, as seen below the P- and S-wave arrivals.

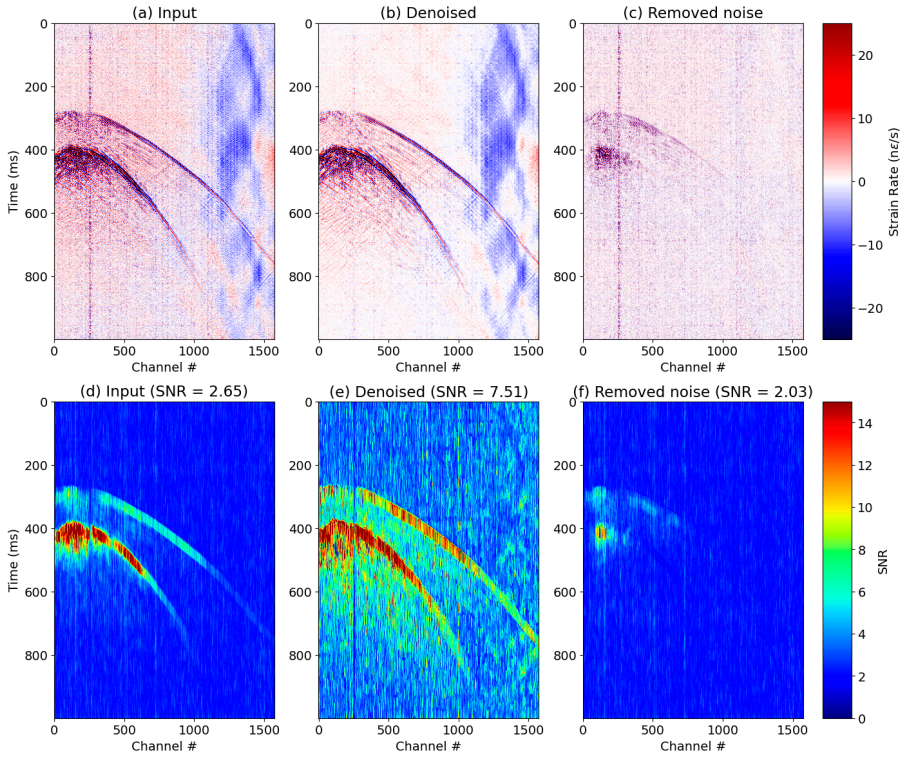


Figure 13. Denoising performance of the SL neural network on an example of the microseismic DAS data: (**a**) input data, (**b**) denoised result and (**c**) removed noise. To quantitatively assess denoising ability, SNR sections are computed for (**d**) input data, (**e**) denoising results and (**f**) removed noise. The average SNR values are displayed at the top of each section.

A comparison of SNR sections before and after noise reduction (Figure 13d,e) highlights the improved coherence of the principal wave components. Figure 13c,f display the noise removed from the original data and the accompanying SNR section. In the removed noise, we still observe coherent signal components, which will be subject to further discussion in the next section.

3.3.2. Noise2Noise Trained Neural Network

Figure 14a shows the raw DAS record of the microseismic event acquired in Otway (the same as Figure 13a), while Figure 14b,c show the denoised and removed noise sections obtained after applying the N2N-trained denoising neural network. Similar to the results obtained with the SL approach, we observe a clear noise reduction and enhancement of low-amplitude signals, as shown in Figure 14b. However, we notice a rather strong signal leakage on the denoised section (Figure 14b) and the SNR attribute section of the denoised result (Figure 14e). This may be partly attributed to the fact that the N2N-trained neural network improves upon the five m spatial resolution inherent to the use of constellation fiber, as shown in the close-up sections of the event (Figure 15). This is enabled by the fact that the neural network was trained on a standard fiber with 1 m channel spacing and could potentially explain part of the signal leakage observed in the removed noise section (Figure 14c).

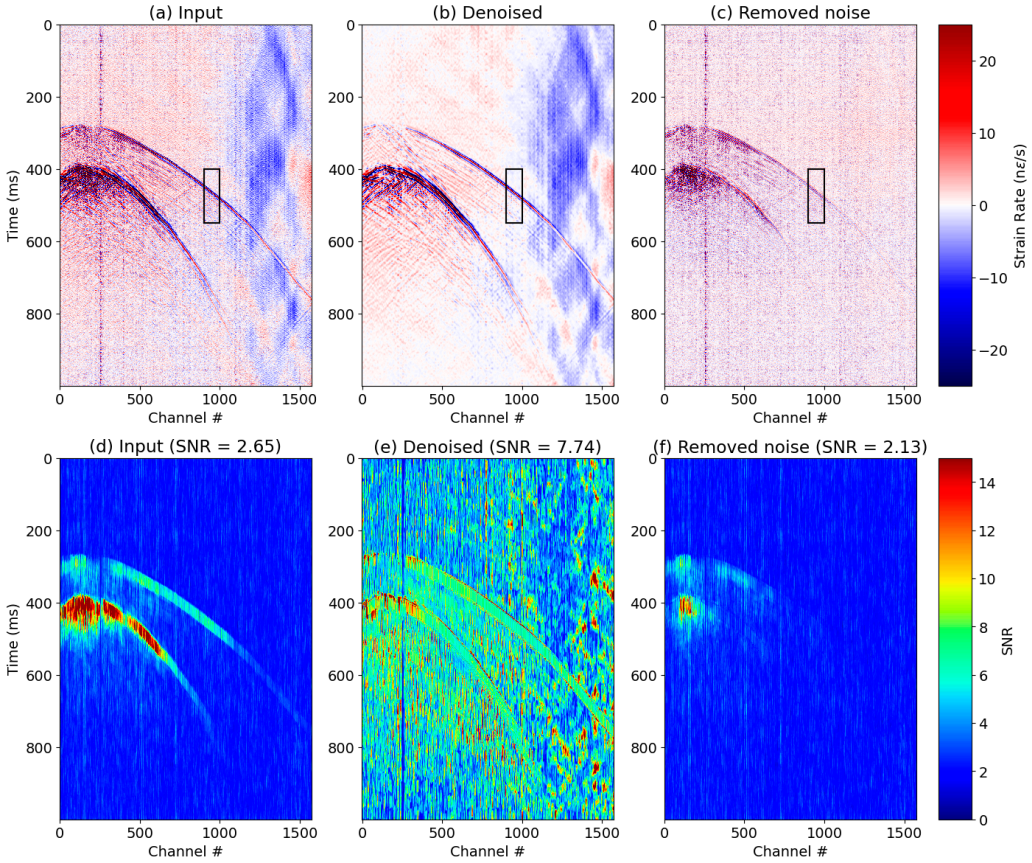


Figure 14. Denoising performance of the N2N-trained neural network on a microseismic event recorded in Otway CRC-7 well: (**a**) input, (**b**) denoised result and (**c**) removed noise. The black rectangles delineate the magnified sections shown in Figure 11. Corresponding SNR attribute sections are shown in panels (**d**–**f**). The average SNR values are displayed at the top of each section.

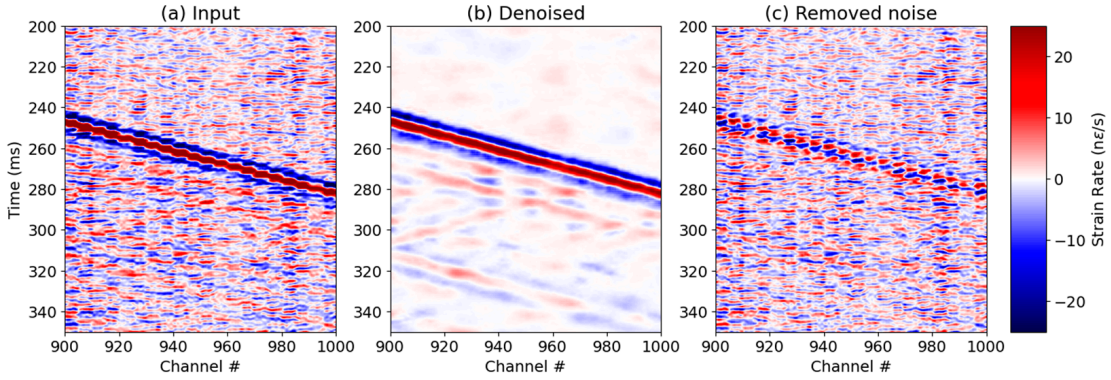


Figure 15. Magnified sections of denoising results of the N2N-trained neural network on a microseismic event recorded in Otway CRC-7 well: (**a**) input, (**b**) denoised result and (**c**) removed noise.

4. Discussion

The aim of this study is to test two deep learning denoising approaches to remove DAS instrumental noise. As illustrated in Figure 1, this noise is a mixture of random noise and high-intensity noise apparent on contiguous channels (vertical streaks). This noise significantly affects the quality of seismic records, especially shot gathers acquired with low-power active sources (Figure 9a) and records of low-magnitude microseismic events. Hence, suppressing DAS instrumental noise could facilitate and speed up DAS VSP surveys acquired with low-energy sources by lowering the number of shot repetitions required to produce high-quality data [28]. In addition, efficient tools to suppress this noise could aid in the real-time detection of microseismicity.

The two investigated approaches both have benefits and limitations. The obvious advantage of the N2N approach is the training of the neural network on field data, which lifts the requirement for building a training dataset comprising clean/noisy data pairs and limits the risk of data mismatch when applying the neural network to field data. Building the training dataset, however, requires access to DAS data with specific acquisition geometries (e.g., spliced fibers or fiber-optic cables looped at the bottom of a wellbore). Another limitation emphasized by this work is that the risk of data mismatch may not be fully addressed if the frequency bands of the training and application data are different. On the other hand, with the SL approach, we have more control over the training dataset, including the frequency bandwidth and the levels of noise. In addition, this method can be adapted to other types of noises by adding ambient noise records instead of instrumental noise to the synthetic dataset; this is, however, outside the scope of this study. The main complexity of the SL approach is building a sufficiently realistic dataset in terms of noise and signal.

To further highlight the differences in the results obtained using the SL and N2N pre-trained denoising neural networks, we show the denoised sections and removed noise sections of the Otway microseismic event in Figure 16a,b and Figure 16e,f, respectively. Even though the average SNR value for the N2N approach is slightly larger than for the SL approach (7.66 vs. 7.58), there seems to be a significant signal leakage for the N2N approach compared to the SL approach, as illustrated in Figure 16e,f. As discussed above, this signal leakage could be due to the five meters interpolation that the N2N neural network is performing. To confirm this hypothesis, we show close-up sections of the P-wave arrival in Figure 17a,b for the denoised results obtained using the N2N and the SL approaches, respectively. We note that N2N is effective in removing the 5 m steps compared to the other approach.

The higher signal leakage observed for N2N is also partly caused by the loss of high frequencies, as discussed earlier when analyzing the denoising performance of the N2N-trained neural network on the semi-synthetic dataset. To highlight the dependence of the N2N approach on the training dataset, we trained a N2N denoising network on pairs made of the synthetics used for the SL approach (generated with a 160 Hz central frequency

Ricker wavelet) and two different noise realizations. We then compared its denoising results (Figure 18a,d) to those of the SL model trained with the same high-frequency semi-synthetic data (Figure 18b,e). The results indicate that both methods perform similarly on microseismic data when trained on semi-synthetic data with the same frequency band. Additionally, to assess the impact of the training data frequency on denoising effectiveness, Figure 18c,f display the results of the SL model trained on low-frequency semi-synthetic data, generated by a Ricker wavelet with a central frequency of 100 Hz. Since high-frequency components are absent in the training data, there is an increase in signal leakage, demonstrating that the frequency content of the training data frequency greatly impacts the performance of denoising neural networks. The SL approach uses training data with higher-frequency content, which could explain its better performance, especially in the high-frequency range. Consequently, the N2N may not yield satisfactory results if trained on signals with a frequency content significantly different from the frequency content of the application data.

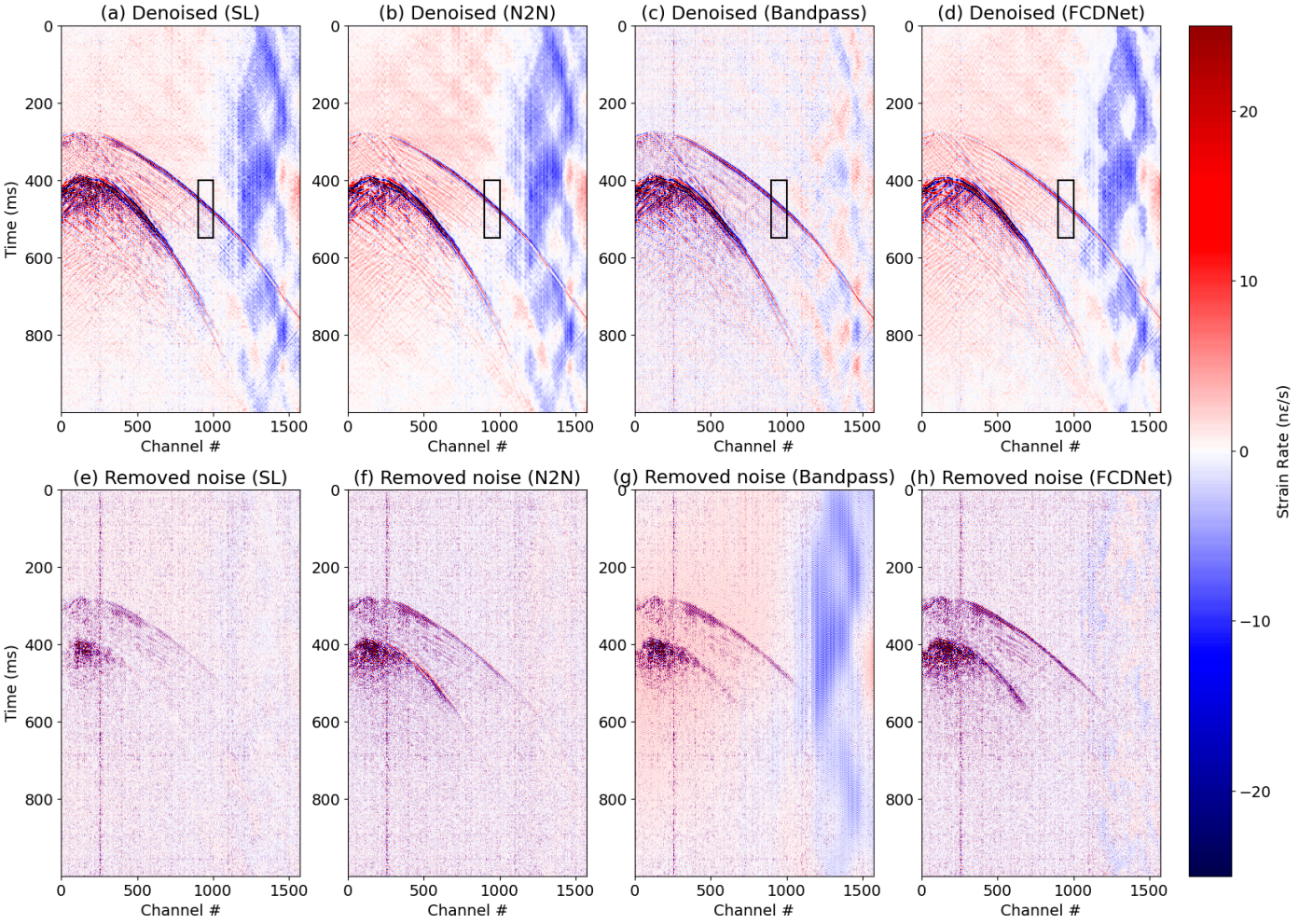


Figure 16. Comparison of the denoising results obtained for the microseismic event recorded in Otway CRC-7 well using (**a**,**e**) the SL approach, (**b**,**f**) N2N trained neural network, (**c**,**g**) bandpass filtering and (**d**,**h**) FCDNet. The upper row shows the denoised sections, while the lower row shows the removed noise sections. The black rectangles in panels (**a**–**d**) delineate the magnified sections shown in Figure 17.

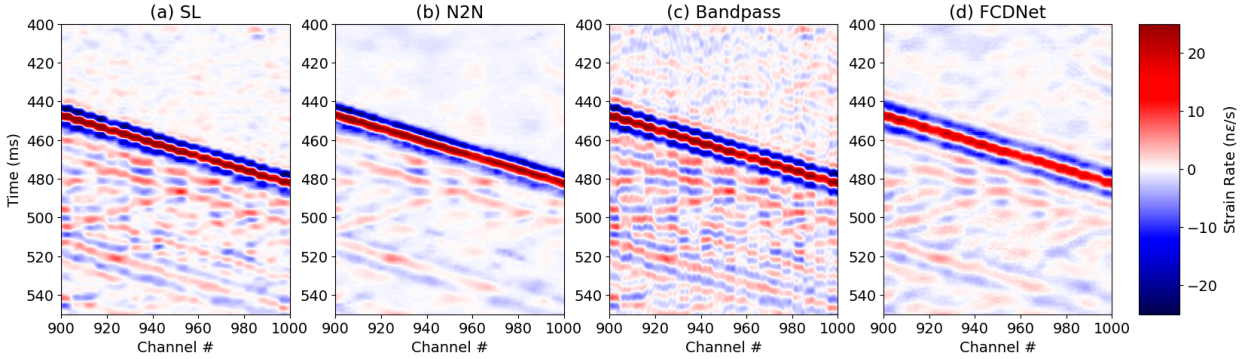


Figure 17. Magnified sections of the denoised results obtained using (**a**) the SL-trained neural network, (**b**) the N2N-trained neural network, (**c**) bandpass filtering and (**d**) FCDNet for the microseismic event recorded in Otway CRC-7 well.

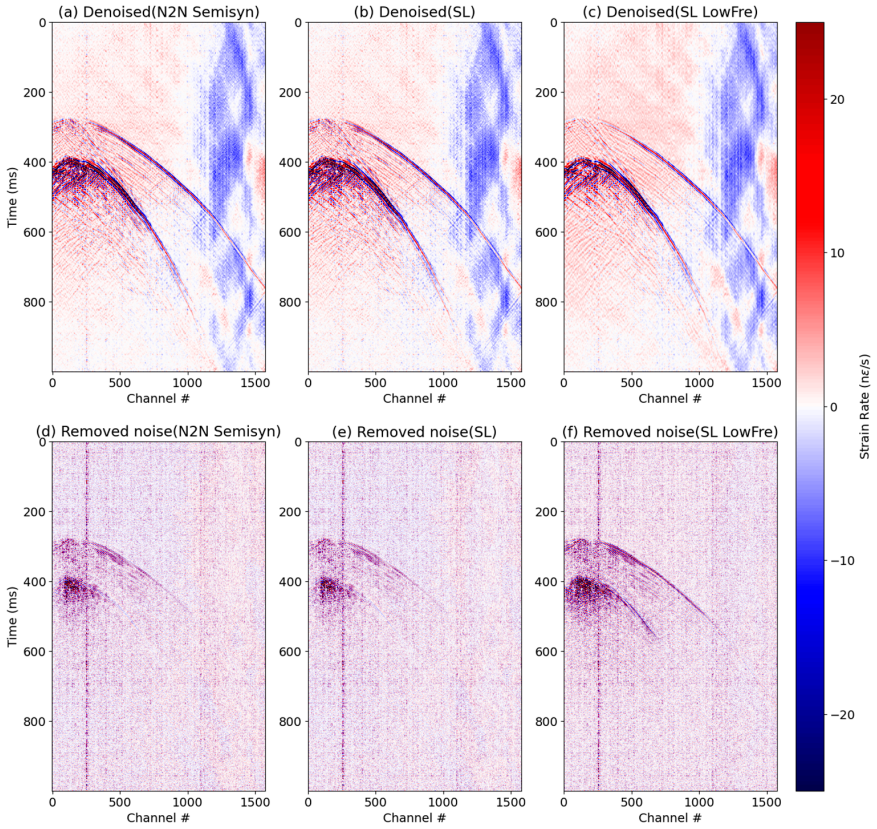


Figure 18. Comparison between (**a**,**d**) N2N trained with high-frequency semi-synthetic data, (**b**,**e**) the SL approach trained with high-frequency semi-synthetic data (160 Hz Ricker wavelet) and (**c**,**f**) the SL approach trained with lower frequency band semi-synthetic data (100 Hz Ricker wavelet). The upper row shows the denoised sections, while the lower row shows the removed noise sections.

To further demonstrate the efficacy of our denoising neural networks, we used two benchmark models for comparison: a conventional bandpass filter and FCDNet, a neural network trained using artificial noise. The bandpass filter consisted of an Ormsby filter with cut-off frequencies set to 1, 5, 100, and 200 Hz. The optimal training model for DAS denoising using FCDNet was obtained from Yang et al. [17]. Note that this model was not re-trained on field data for this application. Figure 16c,d show the denoising results obtained on Otway microseismic data using bandpass filtering and FCDNet, respectively, while Figure 16g,h show the corresponding removed noise sections and our training model, respectively. In comparison to the other SL method, it is evident that bandpass filtering

leaves the most residual noise in the denoised data. FCDNet exhibits the capability to eliminate most of the complex DAS noise. However, it significantly compromises useful seismic signals during the denoising process, with the signal leakage in the removed noise section being the most prominent compared to the other three methods. This probably results from the neural network training on denoised/noisy data, with a denoising routine not suitable to this particular dataset.

The DAS-N2N denoising approach was previously applied to data acquired for the Rutford Ice Stream in Antarctica [23]. Figure 19 shows a comparison of the denoising results obtained with the current DAS-N2N network and the original DAS-N2N network from Lapins et al. [23]. The data denoised from the original DAS-N2N network suffers from an amplitude dimming, which stands out on the P-wave and S-wave first arrivals. As argued by Lapins et al., this weaker signal amplitude could be due to the fact that the neural network was trained on very noisy data or large portions of passive data containing no seismic events. This signal leakage issue is commonly observed with denoising methods based on mean absolute error (MAE) and MSE loss functions (e.g., [37]). Nonetheless, this comparison illustrates the versatility of this method. Indeed, the current DAS-N2N approach was trained on the active seismic data acquired, but it still generalizes well to passive data, while the original DAS-N2N was trained on surface passive data, but it still applies to passive and active data acquired downhole. As such, the denoising N2N networks can be trained on both passive and active datasets. Adding more variety to the training data, in terms of frequency content, for instance, could greatly improve the performance of the N2N approach. This will be tested in further studies.

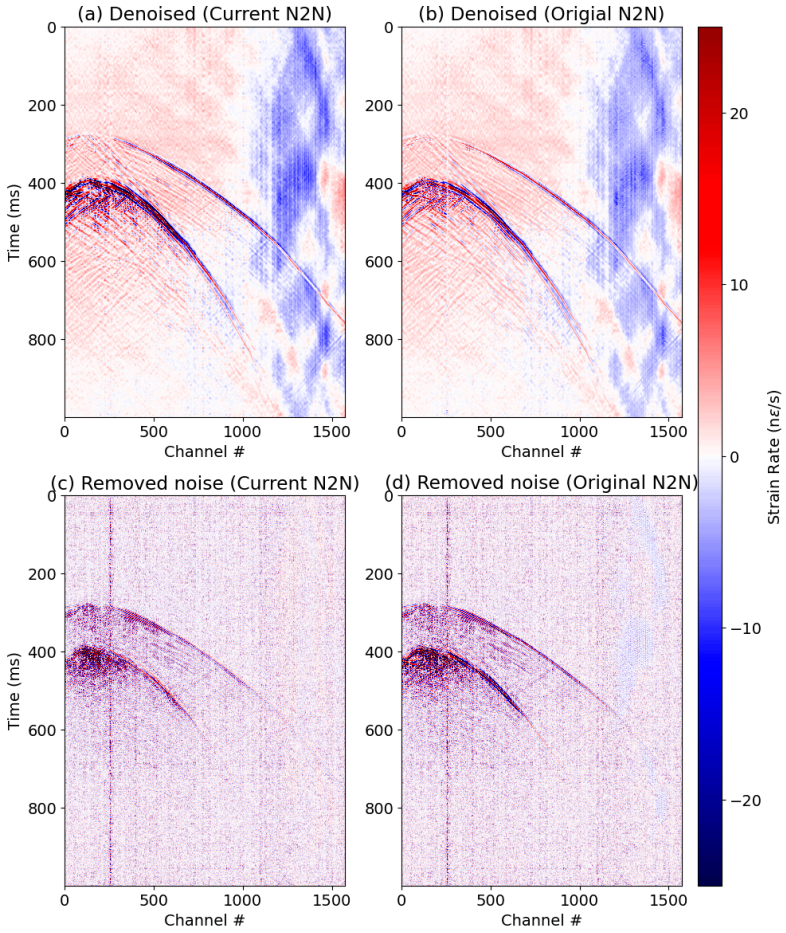


Figure 19. Comparison between the current N2N-trained network (**a**,**c**) and the original DAS-N2N network trained by Lapins et al. [23] (**b**,**d**). Figure (**a**,**b**) show the denoised sections, while figure (**c**,**d**) show the removed noise sections.

Last but not least, the SL and N2N approaches apply to any interrogator, provided the neural networks are re-trained on noise recorded on this specific type of interrogator with similar acquisition settings. This opens the way for rapid, efficient and instrument-specific DAS denoising.

5. Conclusions

This study presents a comparison between two deep learning approaches to address DAS hardware noise and enhance the quality of DAS data. These approaches have the advantage of including real instrumental noise in the neural network training dataset. For the SL approach, real DAS instrumental noise measured on an acoustically isolated coil is added to synthetic data to generate training pairs of clean/noisy data. For the second method, the N2N approach, the training is performed on noisy/noisy data pairs recorded simultaneously on the downgoing and upgoing parts of a downhole fiber-optic cable. The application of the N2N denoising method on other semi-synthetic and field datasets demonstrates the effectiveness of the trained neural networks in attenuating the instrument noise. Both approaches allow us to remove the unwanted noise that lies within the same frequency band of the useful signal, a result that cannot be achieved by conventional denoising techniques employing frequency filtering. The newly trained neural networks also compare favorably with FCDNet, a neural network trained on denoised field data. The advantage of using the SL method over the N2N method and vice versa mainly depends on how representative the training dataset is compared to the application dataset. In this study, we showed that the frequency content of the training dataset greatly impacts the results.

Author Contributions: Conceptualization, O.C., K.T. and R.P.; methodology, X.G., O.C. and R.P.; software, X.G., O.C. and R.P.; validation, X.G. and O.C.; formal analysis, X.G. and O.C.; investigation, X.G., O.C., K.T. and R.P.; resources, K.T. and R.P.; data curation, X.G., O.C., K.T. and R.P.; writing—original draft preparation, X.G. and O.C.; writing—review and editing, K.T. and R.P.; visualization, X.G. and O.C.; supervision, O.C., K.T. and R.P.; project administration, K.T. and R.P.; funding acquisition, K.T. and R.P. All authors have read and agreed to the published version of the manuscript.

Funding: The work was supported by the Mineral Exploration Cooperative Research Centre whose activities are funded by the Australian Government's Cooperative Research Centre Program. This is MinEx CRC Document 2024/36. This research was also funded by the Department of Industry Innovation and Science through the 2021 Global Innovation Linkage, grant number GILIII000114. The authors are grateful for financial support from sponsors at the Curtin Reservoir Geophysics Consortium (CRGC). Xihao Gu acknowledges the support of the China Scholarship Council State Scholarship Fund (202206450061).

Data Availability Statement: All the codes are written in Python, and the codes and data needed to reproduce the shown results are available on Github (https://github.com/CEGCurtin/DASDenoisingML_RemoteSensing, accessed on 7 November 2011). The corresponding author may be contacted, if need be, concerning access to the full training datasets used in the project.

Acknowledgments: The authors would like to thank Tariq Alkhalifah and Claire Birnie for their inspiring discussions and Boris Gurevich and Pavel Shashkin for their constructive feedback. The authors would also like to thank CO2CRC for their permission to show the data.

Conflicts of Interest: The authors declare no conflicts of interest.

References

1. Hartog, A.H. *An Introduction to Distributed Optical Fibre Sensors*; CRC Press: Boca Raton, FL, USA, 2017.
2. Ajo-Franklin, J.B.; Dou, S.; Lindsey, N.J.; Monga, I.; Tracy, C.; Robertson, M.; Rodriguez Tribaldos, V.; Ulrich, C.; Freifeld, B.; Daley, T.; et al. Distributed acoustic sensing using dark fiber for near-surface characterization and broadband seismic event detection. *Sci. Rep.* **2019**, *9*, 1328. [CrossRef] [PubMed]
3. Correa, J.; Pevzner, R.; Freifeld, B.M.; Robertson, M.; Daley, T.M.; Wood, T.; Tertyshnikov, K.; Yavuz, S.; Glubokovskikh, S. Continuous Downhole Seismic Monitoring Using Surface Orbital Vibrators and Distributed Acoustic Sensing at the CO2CRC Otway Project: Field Trial for Optimum Configuration. *Geophys. Monogr. Ser.* **2021**, *268*, 175–189. [CrossRef]

4. Daley, T.M.; Freifeld, B.M.; Ajo-Franklin, J.; Dou, S.; Pevzner, R.; Shulakova, V.; Kashikar, S.; Miller, D.E.; Goetz, J.; Henninges, J.; et al. Field testing of fiber-optic distributed acoustic sensing (DAS) for subsurface seismic monitoring. *Lead. Edge* **2013**, *32*, 699–706. [CrossRef]
5. Lellouch, A.; Lindsey, N.J.; Ellsworth, W.L.; Biondi, B.L. Comparison between distributed acoustic sensing and geophones: Downhole microseismic monitoring of the FORGE geothermal experiment. *Seismol. Soc. Am.* **2020**, *91*, 3256–3268. [CrossRef]
6. Klaasen, S.; Paitz, P.; Lindner, N.; Dettmer, J.; Fichtner, A. Distributed Acoustic Sensing in Volcano-Glacial Environments—Mount Meager, British Columbia. *J. Geophys. Res. Solid Earth* **2021**, *126*, e2021JB022358. [CrossRef]
7. Bellefleur, G.; Schetselaar, E.; Wade, D.; White, D.; Enkin, R.; Schmitt, D.R. Vertical seismic profiling using distributed acoustic sensing with scatter-enhanced fibre-optic cable at the Cu–Au New Afton porphyry deposit, British Columbia, Canada. *Geophys. Prospect.* **2020**, *68*, 313–333. [CrossRef]
8. Correa, J.; Egorov, A.; Tertyshnikov, K.; Bona, A.; Pevzner, R.; Dean, T.; Freifeld, B.; Marshall, S. Analysis of signal to noise and directivity characteristics of DAS VSP at near and far offsets—A CO2CRC Otway Project data example. *Lead. Edge* **2017**, *36*, 994a1–994a7. [CrossRef]
9. Lindsey, N.J.; Rademacher, H.; Ajo-Franklin, J.B. On the broadband instrument response of fiber-optic DAS arrays. *J. Geophys. Res. Solid Earth* **2020**, *125*, e2019JB018145. [CrossRef]
10. Lellouch, A.; Schultz, R.; Lindsey, N.J.; Biondi, B.; Ellsworth, W.L. Low-magnitude seismicity with a downhole distributed acoustic sensing array—Examples from the FORGE geothermal experiment. *J. Geophys. Res. Solid Earth* **2021**, *126*, e2020JB020462. [CrossRef]
11. Atterholt, J.; Zhan, Z.; Shen, Z.; Li, Z. A unified wavefield-partitioning approach for distributed acoustic sensing. *Geophys. J. Int.* **2022**, *228*, 1410–1418. [CrossRef]
12. Ibrahim, A.D.A.; Lin, S.; Xiong, J.; Jiang, J.; Fu, Y.; Wang, Z. Integrated principal component analysis denoising technique for phase-sensitive optical time domain reflectometry vibration detection. *Appl. Opt.* **2020**, *59*, 669–675. [CrossRef] [PubMed]
13. Chen, J.; Ning, J.; Chen, W.; Wang, X.; Wang, W.; Zhang, G. Distributed acoustic sensing coupling noise removal based on sparse optimization. *Interpretation* **2019**, *7*, T373–T382. [CrossRef]
14. Chen, Y.; Savvaidis, A.; Fomel, S.; Chen, Y.; Saad, O.M.; Wang, H.; Oboué, Y.A.S.I.; Yang, L.; Chen, W. Denoising of distributed acoustic sensing seismic data using an integrated framework. *Seismol. Soc. Am.* **2023**, *94*, 457–472. [CrossRef]
15. Huang, G.; Bai, M.; Zhao, Q.; Chen, W.; Chen, Y. Erratic noise suppression using iterative structure-oriented space-varying median filtering with sparsity constraint. *Geophys. Prospect.* **2021**, *69*, 101–121. [CrossRef]
16. Guo, Y.; Peng, S.; Du, W.; Li, D. Denoising and wavefield separation method for DAS VSP via deep learning. *J. Appl. Geophys.* **2023**, *210*, 104946. [CrossRef]
17. Yang, L.; Fomel, S.; Wang, S.; Chen, X.; Chen, W.; Saad, O.M.; Chen, Y. Denoising of distributed acoustic sensing data using supervised deep learning. *Geophysics* **2023**, *88*, WA91–WA104. [CrossRef]
18. Batson, J.; Royer, L. Noise2self: Blind denoising by self-supervision. In Proceedings of the 36th International Conference on Machine Learning, Long Beach, CA, USA, 10–15 June 2019; pp. 524–533.
19. Birnie, C.; Ravasi, M.; Liu, S.; Alkhalifah, T. The potential of self-supervised networks for random noise suppression in seismic data. *Artif. Intell. Geosci.* **2021**, *2*, 47–59. [CrossRef]
20. Krull, A.; Buchholz, T.-O.; Jug, F. Noise2void-learning denoising from single noisy images. In Proceedings of the IEEE/CVF Conference on Computer Vision and Pattern Recognition, Long Beach, CA, USA, 15–20 June 2019; pp. 2129–2137.
21. van den Ende, M.; Lior, I.; Ampuero, J.-P.; Sladen, A.; Ferrari, A.; Richard, C. A self-supervised deep learning approach for blind denoising and waveform coherence enhancement in distributed acoustic sensing data. *IEEE Trans. Neural Netw. Learn. Syst.* **2021**, *34*, 3371–3384. [CrossRef] [PubMed]
22. Lehtinen, J.; Munkberg, J.; Hasselgren, J.; Laine, S.; Karras, T.; Aittala, M.; Aila, T. Noise2Noise: Learning Image Restoration without Clean Data. In Proceedings of the 35th International Conference on Machine Learning, ICML, Stockholm, Sweden, 10–15 July 2018; pp. 4620–4631.
23. Lapins, S.; Butcher, A.; Kendall, J.-M.; Hudson, T.S.; Stork, A.L.; Werner, M.J.; Gunning, J.; Brisbourne, A.M. DAS-N2N: Machine learning distributed acoustic sensing (DAS) signal denoising without clean data. *Geophys. J. Int.* **2024**, *236*, 1026–1041. [CrossRef]
24. Welch, P. The use of fast Fourier transform for the estimation of power spectra: A method based on time averaging over short, modified periodograms. *IEEE Trans. Audio Electroacoust.* **1967**, *15*, 70–73. [CrossRef]
25. Pevzner, R.; Glubokovskikh, S.; Isaenkov, R.; Shashkin, P.; Tertyshnikov, K.; Yavuz, S.; Gurevich, B.; Correa, J.; Wood, T.; Freifeld, B. Monitoring subsurface changes by tracking direct-wave amplitudes and traveltimes in continuous distributed acoustic sensor VSP data. *Geophysics* **2022**, *87*, A1–A6. [CrossRef]
26. Schmidt, H.; Jensen, F.B. Efficient numerical solution technique for wave propagation in horizontally stratified environments. *Comput. Math. Appl.* **1985**, *11*, 699–715. [CrossRef]
27. Pielawski, N.; Wählby, C. Introducing Hann windows for reducing edge-effects in patch-based image segmentation. *PLoS ONE* **2020**, *15*, e0229839. [CrossRef] [PubMed]
28. Pevzner, R.; Tertyshnikov, K. DAS facilitates High Quality Offset VSP Data Acquisition with Low Energy Sources. In Proceedings of the 2nd EAGE Workshop on Fiber Optic Sensing for Energy Applications in Asia Pacific, Kuala Lumpur, Malaysia, 5–7 December 2022; pp. 1–5.

29. Zulic, S.; Tertyshnikov, K.; Yurikov, A.; Sidenko, E.; Isaenkov, R.; Pevzner, R. Curtin Geolab Research Facility: Walkaway VSP with DAS and Geophones. In Proceedings of the EAGE Workshop on Fiber Optic Sensing for Energy Applications in Asia Pacific, Online, 9–11 November 2020; pp. 1–5.
30. Ronneberger, O.; Fischer, P.; Brox, T. U-net: Convolutional networks for biomedical image segmentation. In Proceedings of the Medical Image Computing and Computer-Assisted Intervention–MICCAI 2015: 18th International Conference, Munich, Germany, 5–9 October 2015; Proceedings, Part III 18, pp. 234–241.
31. Kingma, D.P.; Ba, J. Adam: A method for stochastic optimization. *arXiv* **2014**, arXiv:1412.6980. [CrossRef]
32. Pang, T.; Zheng, H.; Quan, Y.; Ji, H. Recorrupted-to-recorrupted: Unsupervised deep learning for image denoising. In Proceedings of the IEEE/CVF Conference on Computer Vision and Pattern Recognition, Nashville, TN, USA, 20–25 June 2021; pp. 2043–2052.
33. Hatton, L.; Worthington, M.H.; Makin, J. *Seismic Data Processing: Theory and Practice*; Merlin Profiles Ltd.: Vienna, VA, USA, 1986.
34. Glubokovskikh, S.; Shashkin, P.; Shapiro, S.; Gurevich, B.; Pevzner, R. Multiwell Fiber Optic Sensing Reveals Effects of CO_2 Flow on Triggered Seismicity. *Seismol. Res. Lett.* **2023**, *94*, 2215–2230. [CrossRef]
35. Glubokovskikh, S.; Pevzner, R.; Sidenko, E.; Tertyshnikov, K.; Gurevich, B.; Shatalin, S.; Slunyaev, A.; Pelinovsky, E. Downhole Distributed Acoustic Sensing Provides Insights Into the Structure of Short-Period Ocean-Generated Seismic Wavefield. *J. Geophys. Res. Solid Earth* **2021**, *126*, e2020JB021463. [CrossRef]
36. Ardhuin, F.; Gualtieri, L.; Stutzmann, E.; Nakata, N.; Fichtner, A. Physics of ambient noise generation by ocean waves. *Seism. Ambient. Noise* **2019**, 69–108. [CrossRef]
37. Birnie, C.; Alkhalifah, T. Transfer learning for self-supervised, blind-spot seismic denoising. *Front. Earth Sci.* **2022**, *10*, 1053279. [CrossRef]

Disclaimer/Publisher's Note: The statements, opinions and data contained in all publications are solely those of the individual author(s) and contributor(s) and not of MDPI and/or the editor(s). MDPI and/or the editor(s) disclaim responsibility for any injury to people or property resulting from any ideas, methods, instructions or products referred to in the content.